

.0183

NACA TN 3823

TECH LIBRARY KAFB, NM



0066715

# NATIONAL ADVISORY COMMITTEE FOR AERONAUTICS

TECHNICAL NOTE 3823

## INVESTIGATION OF ROTATING STALL IN A SINGLE-STAGE AXIAL COMPRESSOR

By S. R. Montgomery and J. J. Braun

Massachusetts Institute of Technology



Washington  
January 1957

AFMDC

TECHNICAL NOTE 3823



0066715

## TECHNICAL NOTE 3823

INVESTIGATION OF ROTATING STALL IN A  
SINGLE-STAGE AXIAL COMPRESSOR

By S. R. Montgomery and J. J. Braun

## SUMMARY

The rotating-stall characteristics of a single-stage axial-flow compressor were investigated. The number of stall cells and their propagation velocities were found with and without stator blades. The measured velocities were compared with those predicted by Stenning's theory (see NACA TN 3580), assuming the downstream pressure fluctuations to be negligible, and correlation within 10 percent was obtained at the onset of stall. It was found that the pressure fluctuations caused by rotating stall were less downstream of the rotor than upstream; the minimum reduction across the rotor was 40 percent with stator blades and 75 percent without stator blades. It was also found that, for the compressor tested, the stator blades decreased the number of stall cells and tended to induce rotating stall at larger mass flow rates.

## INTRODUCTION

Rotating stall may be defined as a region of separated flow moving along a blade row. It has been a continuing problem in axial-compressor development because the resulting vibrations cause severe blade stresses to be imposed at low-mass-flow operation. If stall frequencies were predictable, blades could be designed having critical frequencies different from the stall frequency.

Several theories have been put forward for predicting the propagation velocity of a stall cell (refs. 1 to 3). These are all linearized analyses, with Sears and Marble considering the cascade as an actuator disk and Stenning, as a cascade of finite width. A further difference in the theories occurs in connection with the assumption of the downstream flow field; Sears and Marble considered the wakes to mix in zero length, so that the flow field is a continuum, while Stenning also considered the alternative assumption of a series of free jets discharging into a region of constant pressure.

Experimental work has already been conducted on compressors, in particular by Harvard University, the California Institute of Technology, and the National Advisory Committee for Aeronautics (refs. 4 to 6). However, in each instance the work has been carried out on multirow machines, and it appears that considerable interference results from the downstream blade rows.

Since the theories are in variance and the interference due to other blade rows has an unknown effect, the present investigation has been conducted on a single-stage machine, with and without downstream stator blades, in an effort to verify the predicted results with a minimum of interference; however, it was not found possible to remove the inlet guide vanes. The data obtained permit a ready comparison between predicted and actual stall-propagation velocities and, in addition, allow the theoretical models for the downstream flow field to be checked by measurement of the pressure fluctuations.

This investigation was conducted at the Massachusetts Institute of Technology under the sponsorship and with the financial assistance of the NACA.

#### SYMBOLS

A	effective blade passage area
A'	total blade passage area
b	half wave length of stall cell
c	resultant velocity
C <sub>p</sub>	pressure coefficient
c <sub>x</sub>	axial velocity
c <sub>y</sub>	tangential velocity
f	stall-propagation frequency
F	frequency of timing pulse on photographs
L	blade chord length
N	number of stall cells

$p$  separation between inlet guide vanes and rotor  
 $p_s$  static pressure  
 $r$  radius  
 $r_t$  rotor tip radius  
 $U$  rotor velocity at mean radius  
 $V$  stall-propagation velocity at mean radius relative to rotor  
 $w$  inlet velocity relative to rotor  
 $x, y$  coordinate directions  
 $\alpha$  blockage coefficient  
 $\alpha_1$  absolute air angle entering rotor  
 $\alpha_2$  absolute air angle leaving rotor  
 $\beta_1$  air inlet angle relative to rotor  
 $\beta_2$  air outlet angle relative to rotor  
 $\rho$  density  
 $\phi$  perturbation velocity potential

$$\phi_x = \frac{\partial \phi}{\partial x}; \quad \phi_{xx} = \frac{\partial^2 \phi}{\partial x^2}$$

$$\phi_y = \frac{\partial \phi}{\partial y}; \quad \phi_{yy} = \frac{\partial^2 \phi}{\partial y^2}$$

$$\phi_t = \frac{\partial \phi}{\partial t}$$

$\omega$  angular frequency of stall propagation

## EQUIPMENT AND PROCEDURE

## Equipment

The single-stage compressor used in the present investigation is shown in figure 1. It has three blade rows, the inlet guide vanes, rotor blades, and stator blades, each being of "free-vortex" design. The characteristics of this compressor are presented in reference 7.

The compressor dimensions are:

Outside radius, in. . . . .	11.625
Hub-tip ratio . . . . .	0.75
Blade chord length, in. . . . .	1.5
Blade aspect ratio . . . . .	1.9
Pitch-chord ratio at mean radius . . . . .	0.95
Approximate blade-tip clearance, in. . . . .	0.035

Blade angles measured from the axial direction are:

Radius ratio, $r/r_t$	Blade angles, deg, for -					
	Inlet guide vanes		Rotor		Stator	
	Inlet	Outlet	Inlet	Outlet	Inlet	Outlet
0.75	0	28.5	34.8	-2.9	48.9	23.3
.80	0	27.1	38.0	7.1	47.2	22.0
.85	0	25.7	42.9	15.7	46.2	20.6
.90	0	24.4	47.5	23.4	45.1	19.4
.95	0	23.3	51.6	29.7	44.3	18.3
1.00	0	22.2	54.6	34.4	43.3	17.2

The blade profiles were NACA four-digit series 10 percent thick. Figure 2 is a sectional view of the blade region where velocity and pressure measurements were made. An adjustable throttling valve downstream of the blades permitted variation of mass flow.

Qualitative measurements of velocity fluctuations used to indicate the stalled region were obtained by the use of a constant-current hot-wire anemometer (model HWB manufactured by the Flow Corp.). The wire on the probes was tungsten of 0.00035-inch diameter and 0.044 inch long. An additional hot-wire set, locally constructed, was also used when simultaneous indications at different tangential positions were required. The operation of each set is identical and the same size probes were used for each.

The output of the hot-wire anemometers was fed into a dual-beam cathode-ray oscilloscope (type 322 manufactured by the Allen B. Dumont Laboratories, Inc.), which permitted visual observation or photographic recording of the velocity fluctuations. Photographs were obtained with both a still and a strip-film camera, the strip-film camera being employed to include a greater number of stall cells on a single photograph. Representative photographs of each type appear as figures 3 and 4. The time trace included on each velocity-fluctuation photograph was obtained by feeding the output of an audio oscillator into the beam-intensity control of the oscilloscope. The photographic and hot-wire equipment is seen in figure 1.

Pressure fluctuations were measured with a barium titanate crystal, the output of which was fed through an amplifier and thence to the oscilloscope. The pressure taps were located in the outer casing of the compressor before and after each blade row and representative photographs of the pressure fluctuations at various axial positions are shown in figure 5.

A five-hole probe and a sphere probe (manufactured by the Flow Corp.) were used to determine air angles and mean-radius static pressure, respectively. The description of these probes is given in reference 8. The mass flow corresponding to each throttle position was obtained by measuring, with an inclined manometer, the total and static pressure in a calibrated nozzle.

#### Procedure

Runs were conducted at 1,500 rpm both with and without stator blades. This rotational speed was chosen because it gave a maximum axial velocity of 90 feet per second, which satisfied the requirement for incompressible flow. A few runs conducted at a speed 60 percent higher indicated similar stall characteristics, so that the results obtained are representative for the machine over a range of rotational speeds. The various stall regions were obtained by varying the position of the throttle and thereby the mass flow. The changeover from one stall region to another was quite sharp and easily detectable by sound and change in the velocity-fluctuation pattern.

The data recorded in each run were static and total pressure in the calibrated nozzle, photographs of the velocity-fluctuation pattern, and photographs of the pressure fluctuations before and after the rotor and stator. The velocity fluctuations were normally measured at the mean radius, but radial traverses were made to detect any change from root to tip. These data permitted the evaluation of the frequency of the rotating stall, mass flow, and relative magnitude of pressure fluctuations at the various axial positions.

The number of stalled regions was determined by the use of two hot-wire probes, one stationary and one free to traverse tangentially. The wires were initially alined so that the output signals were in phase and one wire was then traversed through a known arc. The relative phase displacement of the stalled region was then correlated with the tangential distance traversed to determine the number of stalled regions.

The rotor performance was obtained by measuring the static pressure and air angles at the mean radius both before and after the blade row, using the sphere and five-hole probes. The pressures were measured with an inclined manometer and data were obtained for mass-flow rates varying from the maximum down to the point where the probe readings became meaningless because of large velocity fluctuations.

## RESULTS

The data were obtained in the form of the steady-state characteristics of the compressor and photographic records from the hot-wire equipment, and the results are presented in figures 6 to 8. From measured values of axial velocity and inlet and outlet angles from the rotor at the mean radius, the angles  $\beta_1$  and  $\beta_2$  of the flow with the rotor were calculated (see fig. 6(a)) using the relations

$$\tan \beta_1 = \frac{U}{c_x} - \tan \alpha_1$$

$$\tan \beta_2 = \frac{U}{c_x} - \tan \alpha_2$$

Hence, knowing the static pressure rise  $\Delta p_s$  measured at the mean radius, the pressure coefficients

$$C_p = \frac{\Delta p_s}{(1/2)\rho w_1^2}$$

were calculated and plotted versus  $\beta_1$  (fig. 6(b)).

Finally, the blockage coefficient  $\alpha$ , as used by Stenning and Emmons to analyze the stability of a propagating wave (refs. 3 and 6), was calculated and plotted versus the cotangent of  $\beta_1$  (fig. 7) where

$$\alpha \approx \frac{A}{A'} = \frac{\cos \beta_1}{\cos \beta_2 \sqrt{1 - C_p}}$$

From the photograph of the hot-wire traces, the frequency of stall propagation was found by using the frequency of the timing pulse or the velocity of the film strip. The number of cells was found from the comparison of phase change with the actual angular displacement of the two probes used, and hence the absolute frequency of a single cell was calculated. Taking the mean radial position as the point of reference, the velocity  $V$  of a single cell relative to that of the rotor can be calculated and is plotted nondimensionally as  $V/c_x$  versus  $\beta_1$  in figure 8.

In addition, the theoretical propagation velocities can be calculated using the theories of Sears (ref. 1) and Marble (ref. 2), which should apply to stall cells of large wave length when the pressure rise across the blade row is small, and also using Stenning's theory (ref. 3), which should be useful for stall cells of small wave length. Since Sears' "airfoil" theory gives unrealistic values of propagation velocity for cells with a wave length very large compared with the blade chord (for which the phase lag must tend to zero), his "channel" theory was employed using the limiting case of zero phase lag. For this case, Sears' and Marble's theories give an identical result:

$$\frac{V}{c_x} = \csc 2\beta_1$$

If a phase lag other than zero is employed in Sears' channel theory, predicted values of  $V/c_x$  are less than  $\csc 2\beta_1$ .

The third theory includes an effect due to the number of stall cells  $N$  and gives the result

$$\frac{V}{c_x} = \frac{2(1 - c_p)}{\sin 2\beta_1 \left[ \frac{L\pi}{b \cos \beta_2} \left( \frac{1 - e^{-2\pi p/b}}{1 + e^{-2\pi p/b}} \right) + 1 \right]}$$

where  $b$  is the half wave length of one cell (Circumference/2N),  $L$  is the chord length, and  $p$  is the separation between the rotor and inlet guide vanes; the expression in the parentheses in the denominator is a correction designed to allow for the effect of the inlet guide vanes on the stall-propagation velocity. These theoretical velocities were calculated from the steady-state characteristics of the compressor and are plotted in figure 8.

## DISCUSSION OF RESULTS

### Steady-State Characteristics

The steady-state characteristics were obtained both with and without the stator blades in position, and excellent agreement was obtained between the observed data. In addition, it was found that without the stator blades it was possible to obtain reasonable data when stall cells of short wave length were present, so that mean data are available for part of the region of rotating stall.

In figures 6(b) and 6(c) where the pressure coefficient is plotted versus  $\beta_1$ , the ranges in which rotating stall occurs are marked both for the stage with stator blades and for that without; a detailed discussion of these regions is given below. It will be noted that there is a rise in pressure coefficient at  $\beta_1 = 66^\circ$ . This was due to the onset of rotating stall, which caused the flow through the stalled blade passages to decrease, while the flow through the unstalled blade passages increased. The net losses across the blade row are apparently reduced, giving an increase in the pressure rise and hence a local rise in pressure coefficient. With stator blades in place no reliable measurement of angles or static pressures is possible when stall begins, since the velocity fluctuations are large.

From stability considerations for a wave propagating in a cascade (refs. 3 and 6) the start of rotating stall is predicted to coincide with the point where a line from the origin is tangent to the curve of the blockage coefficient  $\alpha$  versus cotangent  $\beta_1$ . In figure 7 it is seen that stall propagation does not start until there is a somewhat larger value of  $\beta_1$  than that predicted. This is probably due to the fact that finite fluctuations are involved rather than the small fluctuations assumed in the theoretical model.

### Stall Characteristics With Stator Blades

The first tests were conducted with the stator blades in position, and the following characteristics were observed as the relative inlet angle was increased by decreasing the mass rate of flow.

Four separate regimes of rotating stall were found, the first consisting of one cell at the tips of the blades and the others having one, two, and three cells, respectively, covering the entire blade. Between each regime, a transition state occurred in which the number of cells varied between those found in the adjacent regimes (see fig. 6(b)). The velocity fluctuations were measured at a number of axial positions, and

it was found that the magnitude of the velocity fluctuations decreased with distance both upstream and downstream of the rotor.

The first sign of stall as  $\beta_1$  was increased above the design value was the appearance of random velocity fluctuations, which appeared with increasing regularity until the regime of propagating tip stall was entered. The stalled region extended from the rotor tip for about 3/4 inch down the blade, a distance approximately equal to the thickness of the boundary layer entering the rotor (ref. 7). The number of blades over which the region extended was greatest at the tip and decreased further down the blade, but no actual measurements were made of the number of blades covered by the cell. As  $\beta_1$  was further increased, a single cell was found extending over the entire blade length, and the number of blades covered increased with  $\beta_1$  until the next regime with two stall cells was entered. In the regimes where the entire blade was stalled, neither the velocity-fluctuation pattern nor the number of blades covered varied markedly from root to tip. As  $\beta_1$  was increased, the number of cells increased progressively from one to two to three, a larger number being unobtainable as purely random fluctuations appeared when  $\beta_1$  was greater than  $80^\circ$ , as shown at the bottom of figure 3.

#### Stall Characteristics Without Stator Blades

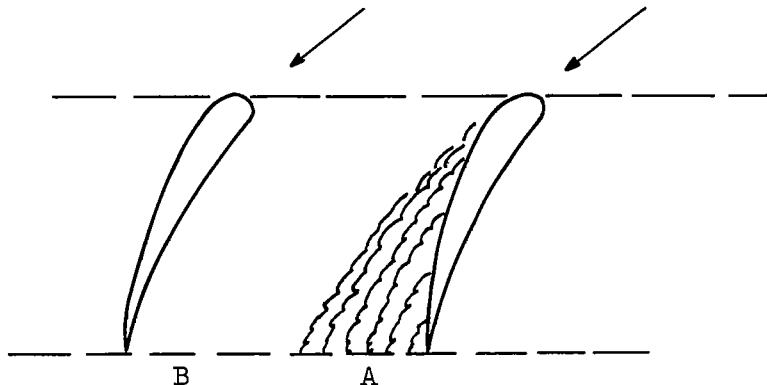
When the stator blades were removed, there was a very marked change in the rotating-stall characteristics; the onset of stall was delayed until a greater value of  $\beta_1$  was reached; and, following the initial regime with random velocity fluctuations, two regimes were found consisting of a much larger number (eight and nine, respectively) of small cells than were obtained with the stator blades in place. On further increase of  $\beta_1$ , the stall characteristics resembled those with the stator blades in place and regimes containing one, three, and four cells were found before random stall reappeared at  $\beta_1 = 85^\circ$ . The regime with two cells appeared as an unstable condition in a very narrow range of inlet angles (fig. 6(c)).

Several striking differences were observed between cells of short and long wave length (high and low frequency). With the former, it was found that the velocity fluctuations were very nearly damped out in the root boundary layer, while the latter showed fluctuations of greater amplitude in the same place. It was also found that, for short wave lengths, the velocity fluctuations measured directly downstream of the rotor at section F in figure 2 were considerably smaller than those at section G. No satisfactory explanation for this has been suggested.

The limits of the various regimes were comparatively well defined when there were a small number of cells, since any change in number caused

an appreciable change in the frequency and in the phase shift between two probes. With eight or nine cells, the problem of determining the actual number becomes more difficult and there is a range of uncertainty between these two regions. Further difficulties are caused by the non-symmetry of the cells around the annulus (fig. 4) and also by the fact that each cell does not cause the same velocity fluctuations at the probe.

Since the blade passages are of finite width, the probe may be at any point across the passage at the instant when the adjacent blade stalls. The process of stalling causes separation from the leading edge of the blade, and there is a reduction of velocity in this region of separated flow (position A in sketch), while the velocity in the unseparated portion of the passage may have an instantaneous increase because of the reduction in flow area (position B).



If the probe is close to the trailing edge of the blade, it may therefore show either an increase or decrease in velocity when stall occurs. Further downstream, mixing has occurred so that each stall cell causes a net decrease in velocity, and, similarly, a probe upstream of the blade row will always indicate a reduction in velocity on account of the partial blockage of the blade passage. The phenomenon was noted for stall cells of short wave length and would be expected when there are only a small number of blade passages covered by each cell.

Finally, it should be noted that a flow reversal will be shown as a velocity increase since a hot wire is nondirectional, and, hence, the midpoint of the cell is sometimes difficult to find on the oscillogram.

#### Comparison of Actual and Predicted Propagation Velocities

As explained above in the section entitled "Results" the experimental points and theoretical curves of propagation velocities are plotted in figure 8. The form in which these figures are presented permits a

comparison of the theoretical and experimental values of the propagation velocities relative to the rotor, and important conclusions can be drawn from them.

First, all the theories are based on the assumption of small perturbations on a steady velocity field and so would be valid only at the onset of rotating stall. Good agreement is obtained at this point with Stenning's theory, both with and without stator blades, while the propagation velocities predicted by the Sears and Marble large-wave-length theories lie below the values observed with stator blades and above those observed without stator blades. At high values of the inlet angle, the velocity fluctuations cannot be considered as small, but all theories give the correct order of magnitude (within about 25 percent) for the propagation velocities if the theoretical curves are extrapolated. It will be noted that throughout the range of available data the velocities predicted by Sears and Marble correspond almost exactly with those predicted by Stenning for four stall cells.

Another striking factor when no stator blades are used is the sudden change from nine cells to a single cell, with a very small change in  $\beta_1$  (fig. 8(b)). The propagation velocity increases by 90 percent when this happens, which would seem to confirm the prediction of Stenning's theory that the propagation velocity is a function of the number of cells and increases with increase of wave length.

A similar result could be deduced from Sears' general theory with the phase lag included because the phase lag is proportional to the ratio of blade time delay to field time delay, and this ratio becomes smaller as the wave length increases.

#### Pressure Fluctuations

In the theoretical analysis of rotating stall, two simple assumptions can be made about the conditions downstream of the blade row. Either the blade passages can be considered as nozzles discharging into a region of constant pressure, or it can be assumed that mixing occurs immediately downstream of the row, so that the downstream flow field is a continuum. These assumptions can readily be checked by measuring the relative magnitude of the upstream and downstream pressure fluctuations and the results of such tests, taken at the outer casing of the compressor, were as follows:

With stator blades in position, it was found that pressure fluctuations were negligible downstream of the stator blades and upstream of the inlet guide vanes as compared with the fluctuations upstream of the rotor. The fluctuations downstream of the rotor were not greatly affected by the onset of rotating stall, but in the extreme condition an appreciable

variation is seen (fig. 5(c)). The upstream fluctuations due to rotating stall were approximately double those downstream of the rotor. It would appear from this that the condition of a constant downstream pressure field, as assumed by Stenning, was not satisfied and therefore the close agreement between theoretical and observed propagation velocities must be considered fortuitous.

Without stator blades, a greater reduction in pressure fluctuations across the rotor was found, as seen in figures 5(d) and 5(e), and the maximum downstream fluctuations due to rotating stall were less than 25 percent of those upstream.

In order to confirm the most suitable assumption for the downstream flow field in the theoretical analyses, an expression for the magnitude of the pressure fluctuations based on Stenning's model of the stall process with the downstream flow field considered as a continuum is calculated in the appendix. The expression obtained is:

$$\frac{\delta p_1}{\delta p_2} = \sqrt{\left(1 - \frac{\tan \beta_1}{V/c_x}\right)^2 + \left[\left(\frac{1 - e^{-2\pi p/b}}{1 + e^{-2\pi p/b}}\right) \frac{1}{V/c_x}\right]^2}$$

From experimental data on the propagation velocities of stall cells without stator blades, the predicted relative magnitude of the pressure fluctuations can be calculated assuming that the downstream flow pattern is continuous. Representative values are given in the following table and can be compared with the observed values in figure 6.

Number of cells . . . . .	8	9	1	3
$\beta$ , deg . . . . .	67.0	73.6	74.6	78.5
$\tan \beta_1$ . . . . .	2.36	3.40	3.63	4.92
$V/c_x$ . . . . .	0.862	1.24	2.32	2.54
$\frac{1 - e^{-2\pi p/b}}{1 + e^{-2\pi p/b}}$ . . . . .	0.825	0.867	0.151	0.413
$\delta p_1/\delta p_2$ . . . . .	1.99	1.88	0.56	0.96

From the observed values of pressure fluctuations without stator blades it can be seen that the actual upstream pressure fluctuations are always greater than four times the downstream fluctuations so that the assumption of a constant pressure field downstream corresponds more closely to the observed results than the assumption of a continuum.

## CONCLUDING REMARKS

From the results obtained from the investigation of rotating stall in a single-stage axial compressor, it can be seen that the propagation velocity has been predicted within 10 percent for a single blade row at the onset of rotating stall using the results of Stenning's theory. Sears' theory could be made to agree with the observed propagation velocity at the beginning of rotating stall by using a suitable value of phase lag, although the pressure rise across the blade row is still quite high, so that the neglect of the factor  $(1 - C_p)$ , where  $C_p$  is the pressure coefficient, in Sear's theory would lead to an erroneous value of phase lag. At high inlet angles relative to the rotor, where the velocity fluctuations become large and the pressure coefficient is small, the actual and predicted velocities agree reasonably well with Stenning's theory and with the results of Sears' and Marble's analyses for cells of large wave length.

It is also seen that the rotating-stall characteristics of the compressor are influenced very strongly by stator blades downstream of the rotor, the effect of this interference being to damp out the propagation of stall cells at high frequencies and to induce stall propagation at higher mass-flow rates.

Finally, measurements of pressure fluctuations upstream and downstream of the rotor when the following stator was removed show that neither of the extreme conditions assumed in the theories for the downstream flow field represents the true state of affairs satisfactorily, although for this particular machine the "free jet" assumption seems closer to the truth than the assumption that mixing occurs in a short distance.

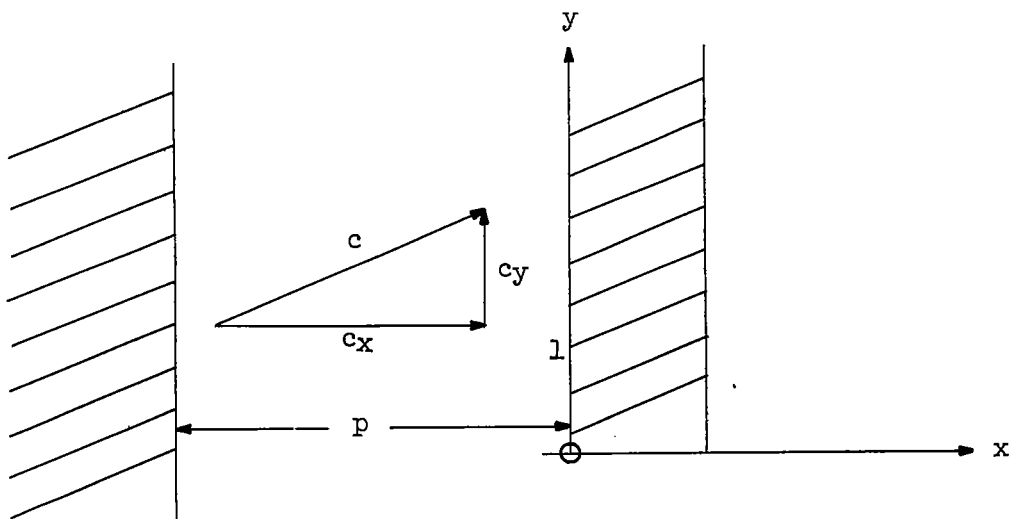
Massachusetts Institute of Technology,  
Cambridge, Mass., June 8, 1955.

## APPENDIX

## PRESSURE FLUCTUATIONS IN A DOWNSTREAM CONTINUUM

The following analysis is designed to estimate the relative magnitude of the upstream and downstream pressure fluctuations caused by rotating stall when the downstream flow field is considered as a continuum.

The analysis is based on the model used by Stenning (ref. 3) shown in the sketch.



For incompressible irrotational flow upstream, a perturbation velocity potential  $\phi$  can be defined, and, from continuity,

$$\phi_{xx} + \phi_{yy} = 0$$

If the rotating stall is considered as a sine wave propagating along the cascade, the solution is

$$\phi = A \sin \left( \frac{\pi y}{b} - \omega t \right) \left[ e^{\pi x/b} + e^{-\pi(x+2p)/b} \right] \quad (1)$$

which satisfies the condition that  $\phi_x = 0$  at  $x = -p$ . This condition allows the interference effect due to upstream guide vanes to be estimated, on the assumption that these guide vanes are closely spaced and of large chord length.

From Euler's equations of motion for unsteady flow with small perturbations, upstream of the cascade (eq. (2) of ref. 3)

$$\phi_t + c \delta c + \frac{\delta p}{\rho} = 0 \quad -\infty < x < 0 \quad (2)$$

Downstream a continuum is assumed (appendix III, ref. 3) and

$$\frac{\delta p_2}{\rho} = (\phi_t)_1 \quad (3)$$

By definition

$$c^2 = c_x^2 + c_y^2$$

therefore

$$c \delta c = c_x \delta c_x + c_y \delta c_y$$

and

$$c_1 \delta c_1 = (c_x \phi_x)_1 + (c_y \phi_y)_1$$

Evaluating equation (2) at point 1 in the preceding sketch and dividing by equation (3),

$$\frac{\delta p_1}{\delta p_2} = \frac{-(\phi_t)_1 - c_1 \delta c_1}{(\phi_t)_1} = \frac{-(\phi_t)_1 - (c_x \phi_x)_1 - (c_y \phi_y)_1}{(\phi_t)_1}$$

Substituting for  $\phi$  from equation (1),

$$\frac{\delta p_1}{\delta p_2} = \frac{\left(1 + e^{-\frac{2\pi p}{b}}\right)\left(\omega - \frac{\pi c_y}{b}\right) \cos\left(\frac{\pi y}{b} - \omega t\right) - \left(1 - e^{-\frac{2\pi p}{b}}\right)\frac{\pi c_x}{b} \sin\left(\frac{\pi y}{b} - \omega t\right)}{\left(1 + e^{-\frac{2\pi p}{b}}\right)\omega \cos\left(\frac{\pi y}{b} - \omega t\right)}$$

Comparing the magnitude of these pressure fluctuations,

$$\left| \frac{\delta p_1}{\delta p_2} \right| = \frac{\sqrt{\left(1 + e^{-2\pi p/b}\right)^2 \left(\omega - \frac{\pi c_y}{b}\right)^2 + \left(1 - e^{-2\pi p/b}\right)^2 \left(\frac{\pi c_x}{b}\right)^2}}{\omega \left(1 + e^{-2\pi p/b}\right)}$$

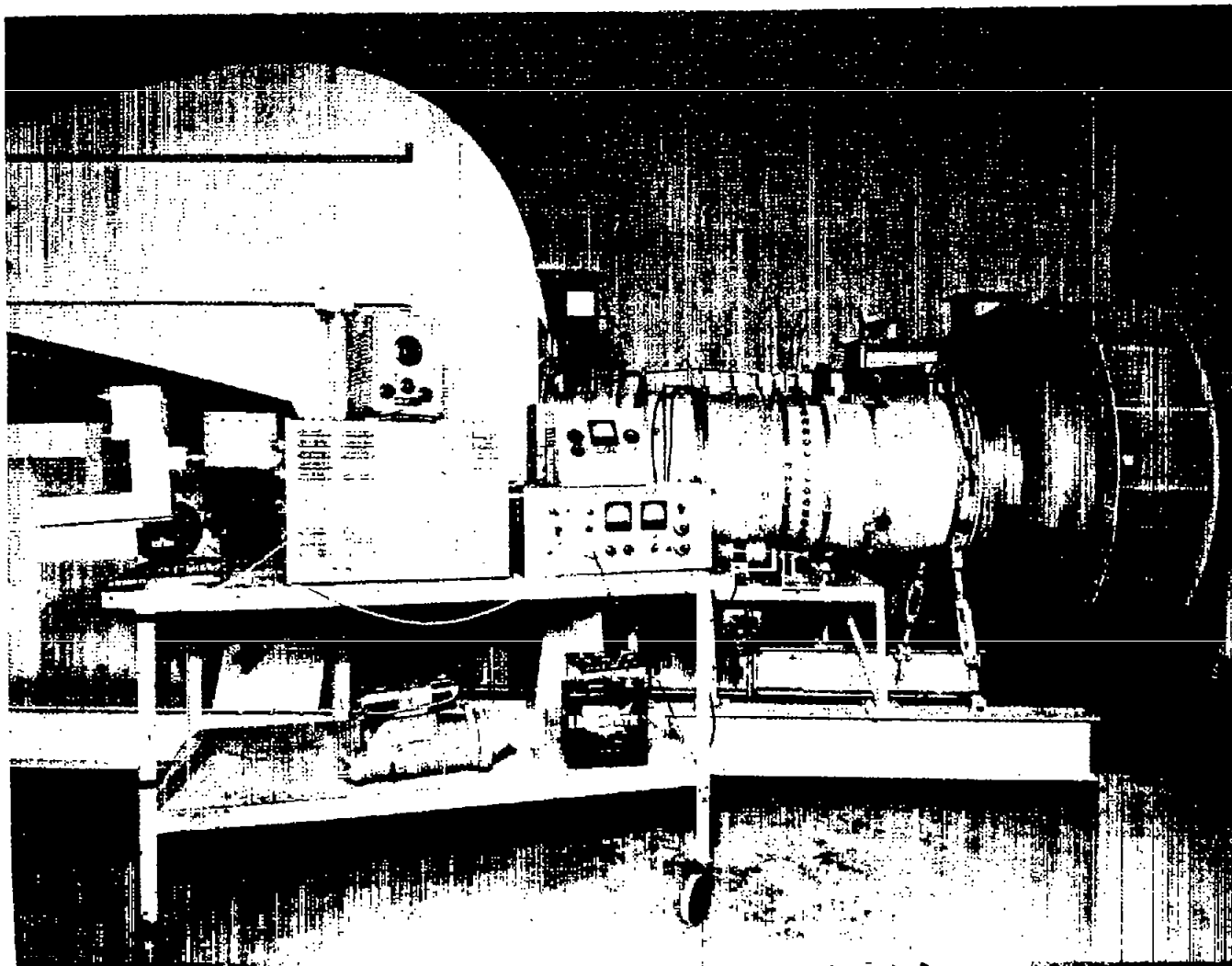
$$= \sqrt{\left(1 - \frac{\pi c_y}{b\omega}\right)^2 + \left(\frac{1 - e^{-2\pi p/b}}{1 + e^{-2\pi p/b}}\right) \left(\frac{\pi c_x}{b\omega}\right)^2}$$

$$= \sqrt{\left(1 - \frac{\tan \beta_1}{V/c_x}\right)^2 + \left(\frac{1 - e^{-2\pi p/b}}{1 + e^{-2\pi p/b}}\right)^2 \left(\frac{1}{V/c_x}\right)^2}$$

This equation shows that the effect of inlet guide vanes is to reduce the ratio of upstream to downstream pressure fluctuations, and it can be used to estimate the theoretical pressure fluctuations with the downstream flow field considered as a continuum.

## REFERENCES

1. Sears, W. R.: A Theory of "Rotating Stall" in Axial Flow Compressors. Contract AF-33(038)21406, Office Sci. Res., U. S. Air Force, and Graduate School Aero. Eng., Cornell Univ., Jan. 1953.
2. Marble, Frank E.: Propagation of Stall in a Compressor Blade Row. Tech. Rep. 4, Contract AF-18(600)-178, U. S. Air Forces and Guggenheim Jet Propulsion Centre, C.I.T., Jan. 1954.
3. Stenning, Alan H., Kriebel, Anthony R., and Montgomery, Stephen R.: Stall Propagation in Axial-Flow Compressors. NACA TN 3580, 1956.
4. Emmons, H. W., Pearson, C. E., and Grant, H. P.: Compressor Surge and Stall Propagation. Paper No. 53-A-56, presented at 1953 annual meeting (Nov. 9-Dec. 3, 1953), A.S.M.E., Dec. 1953.
5. Iura, T., and Rannie, W. D.: Experimental Investigation of Rotating Stall in Axial-Flow Compressors. Trans. A.S.M.E., vol. 76, no. 3, Apr. 1954, pp. 463-471.
6. Huppert, Merle C., and Benser, William A.: Some Stall and Surge Phenomena in Axial-Flow Compressors. Jour. Aero. Sci., vol. 20, no. 12, Dec. 1953, pp. 835-845.
7. Moore, R. W., and Schneider, K. H.: Measurement of Flow Through a Single-Stage Axial Compressor. Rep. 27-6, Gas Turbine Lab., M.I.T., Dec. 1954.
8. Moore, Raymond W., Nelson, Warren G., Prasad, Arun, Richardson, David L., and Turner, James R.: Experimental Techniques for Three-Dimensional Flow Research. Rep. 27-8, Gas Turbine Lab., M.I.T., Dec. 1954.



L-93573

Figure 1.- Apparatus used in investigation.

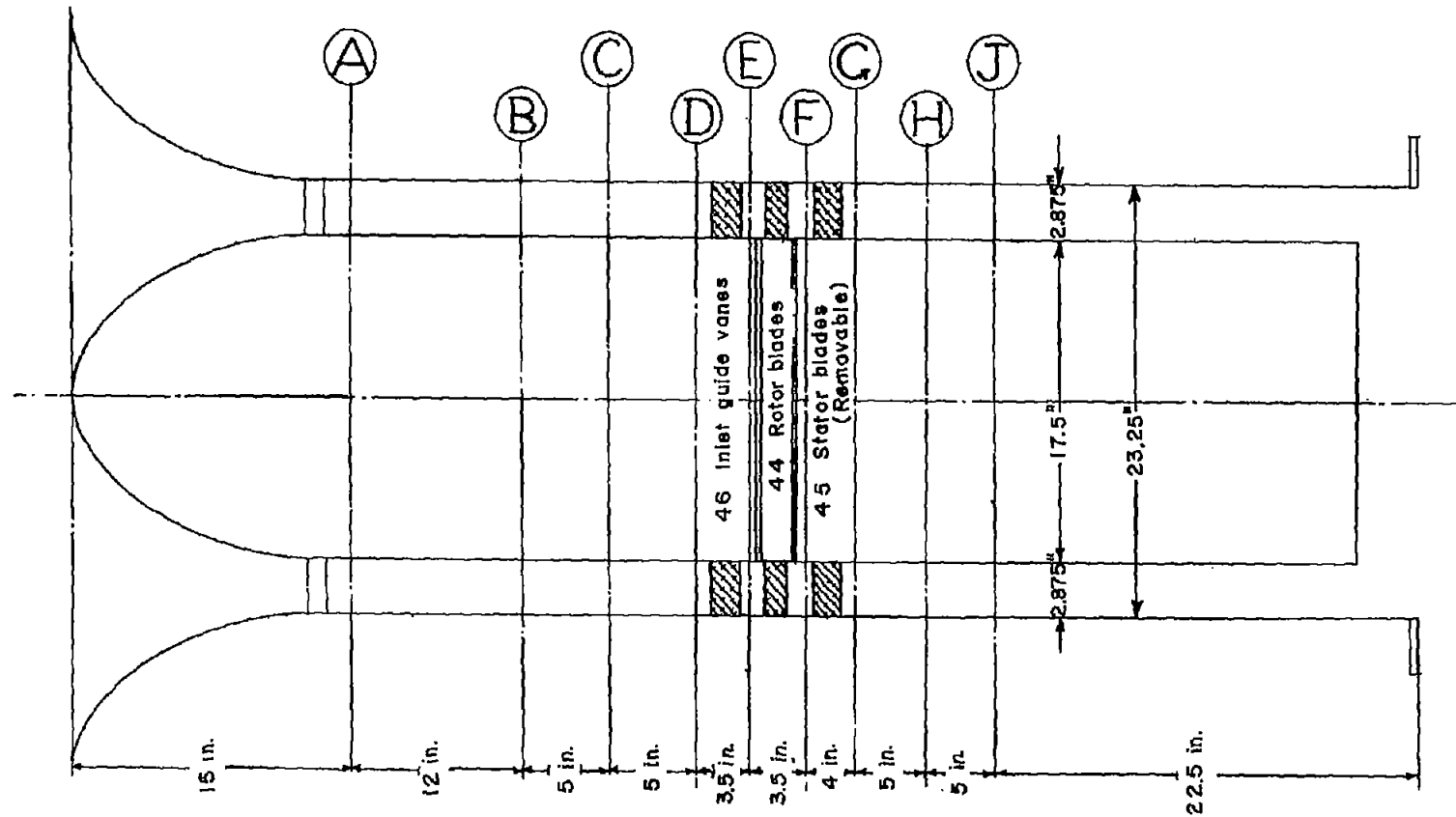


Figure 2.- Schematic diagram of measurement stations of compressor.  
Letters refer to station designations.

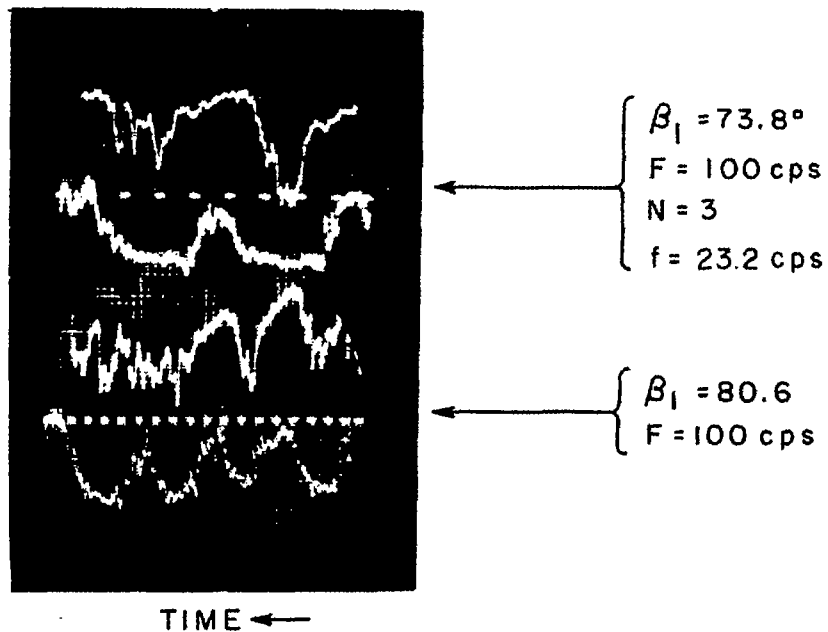
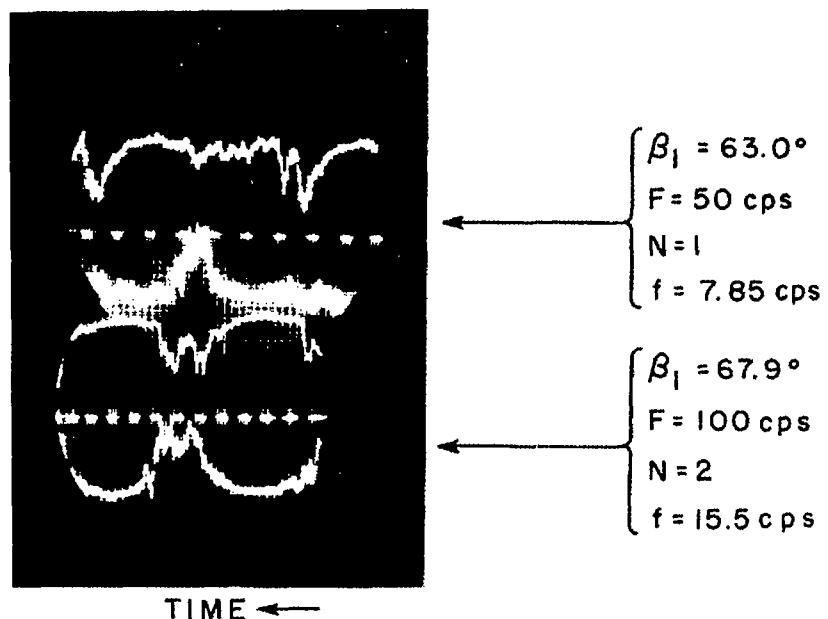


Figure 3.- Velocity fluctuations with stator blades. Velocities decrease toward center of each photograph; probes are downstream of stator and  $180^\circ$  apart.

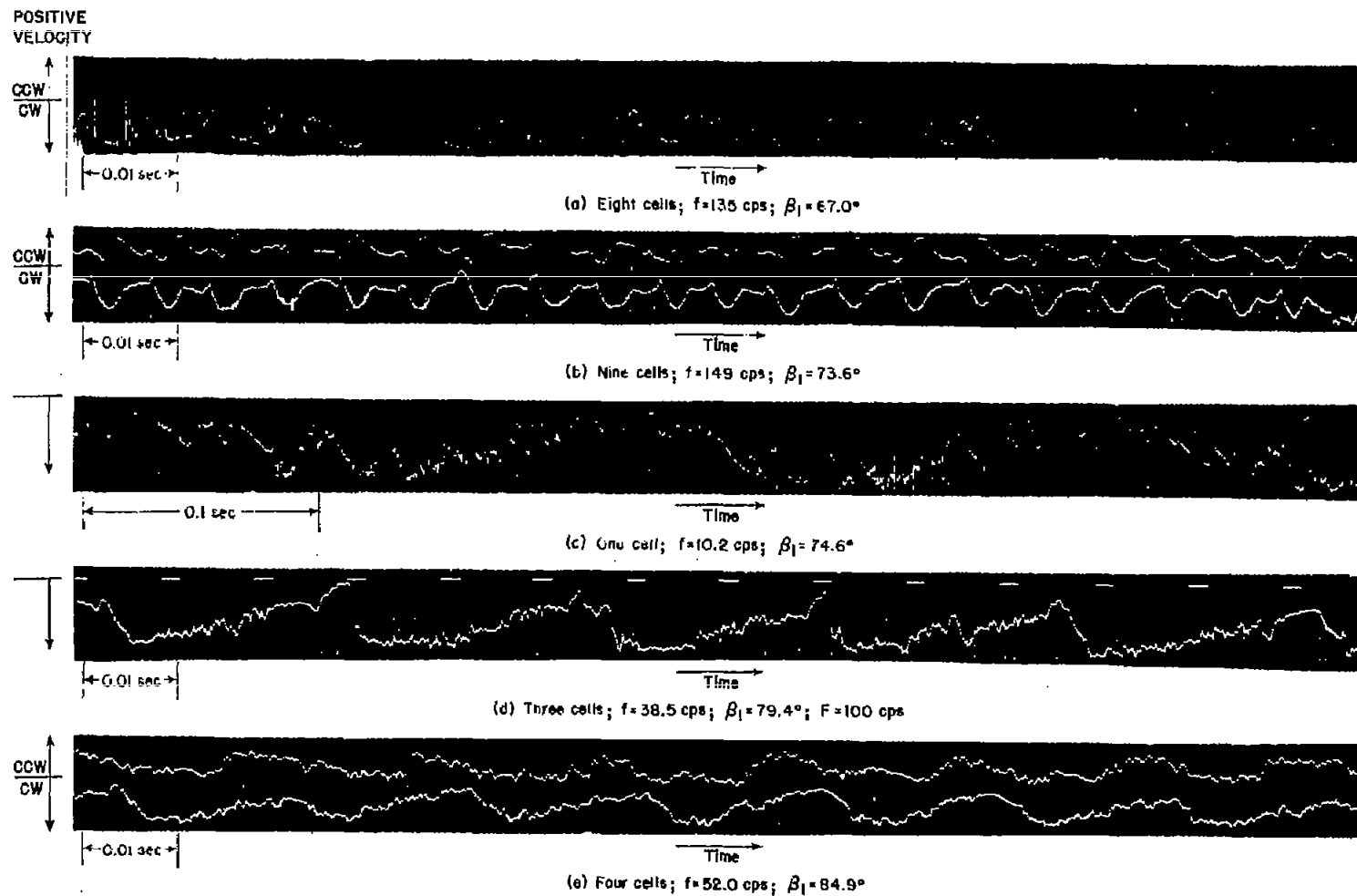


Figure 4.-- Representative strip film records of hot-wire traces without stator blades. Probes are before rotor and  $45^\circ$  apart; clockwise probe receives signal first. CW, clockwise probe; CCW, counterclockwise probe.

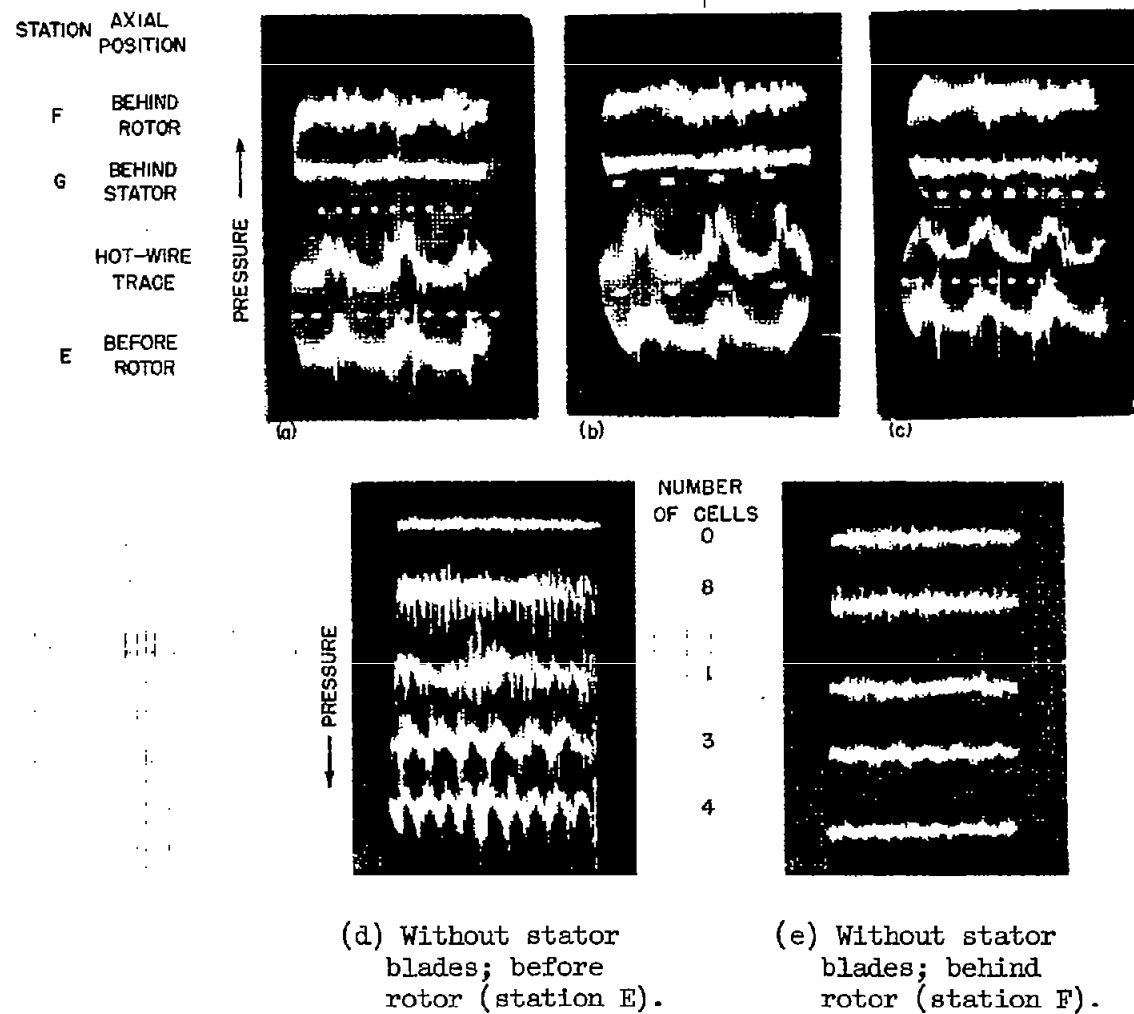


Figure 5.- Static pressure fluctuations. Hot-wire trace is added for comparison in parts (a) to (c).

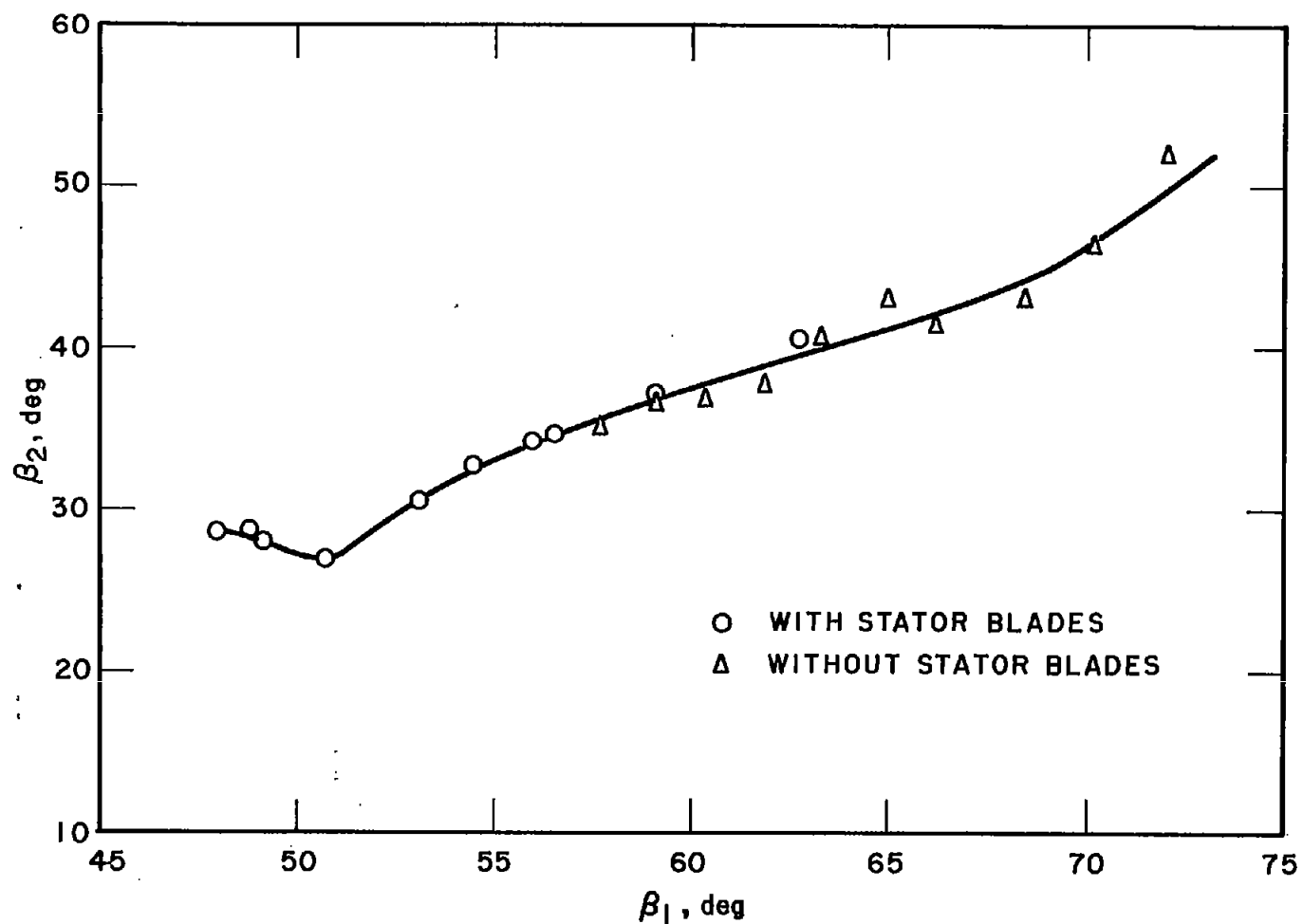
(a)  $\beta_2$  against  $\beta_1$ .

Figure 6.- Rotor performance.

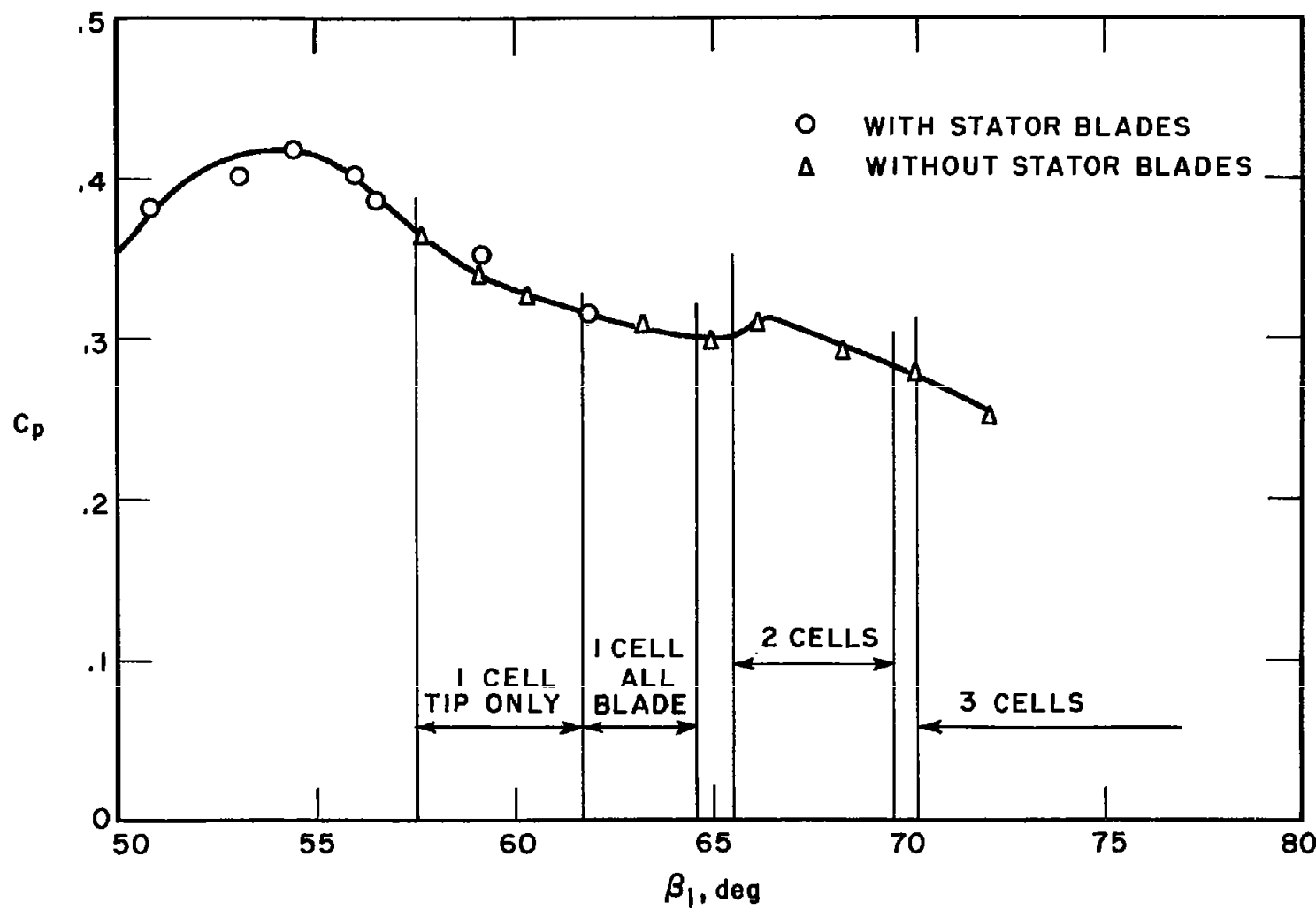
(b)  $C_p$  against  $\beta_1$  showing stall regions with stator blades.

Figure 6.- Continued.

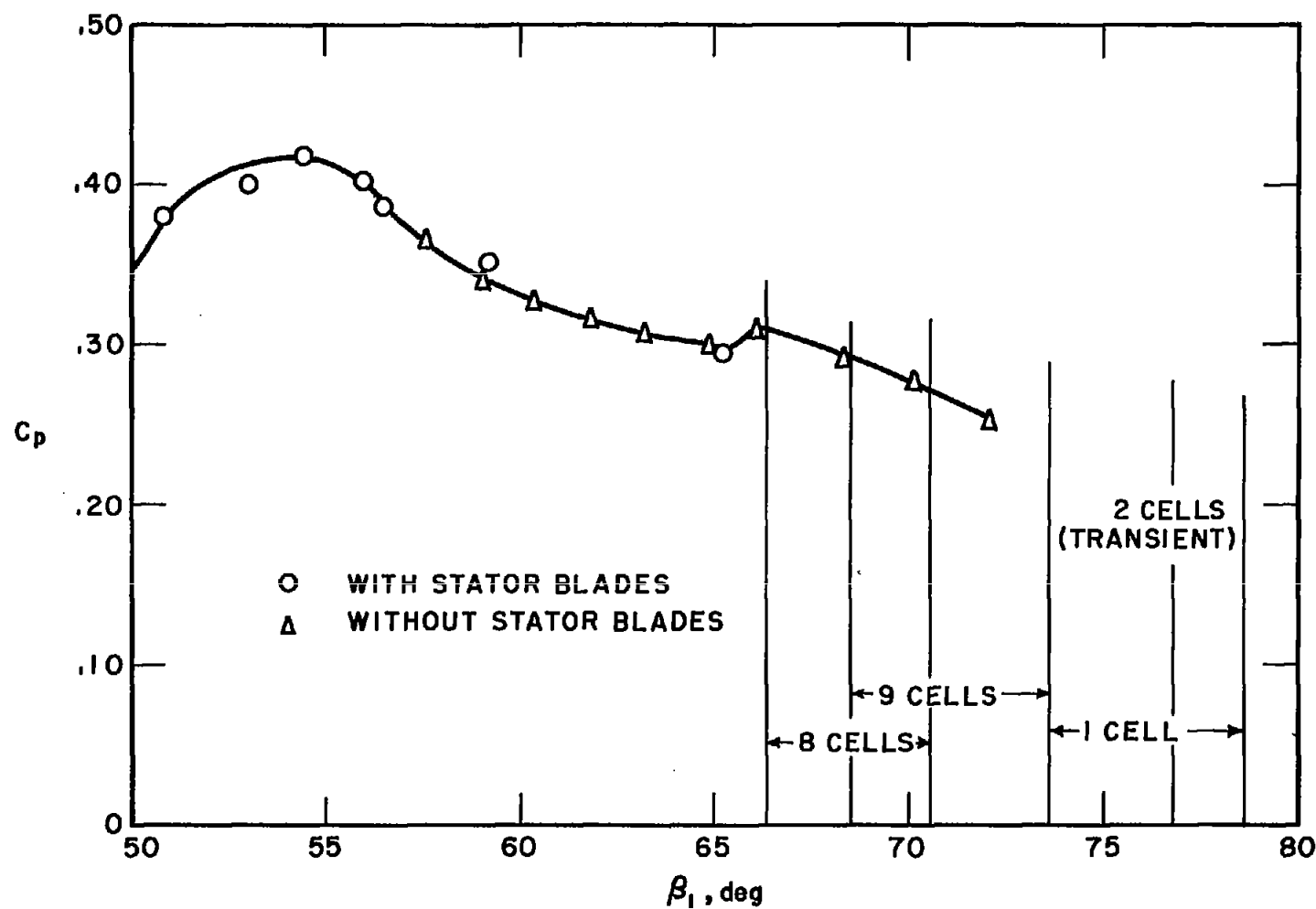
(c)  $C_p$  against  $\beta_1$  showing stall regions without stator blades.

Figure 6.- Concluded.

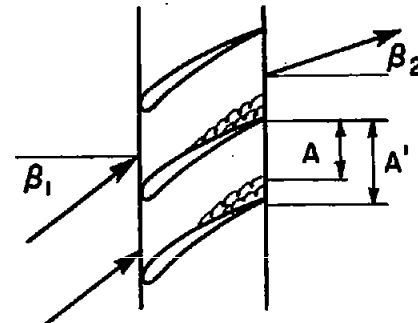
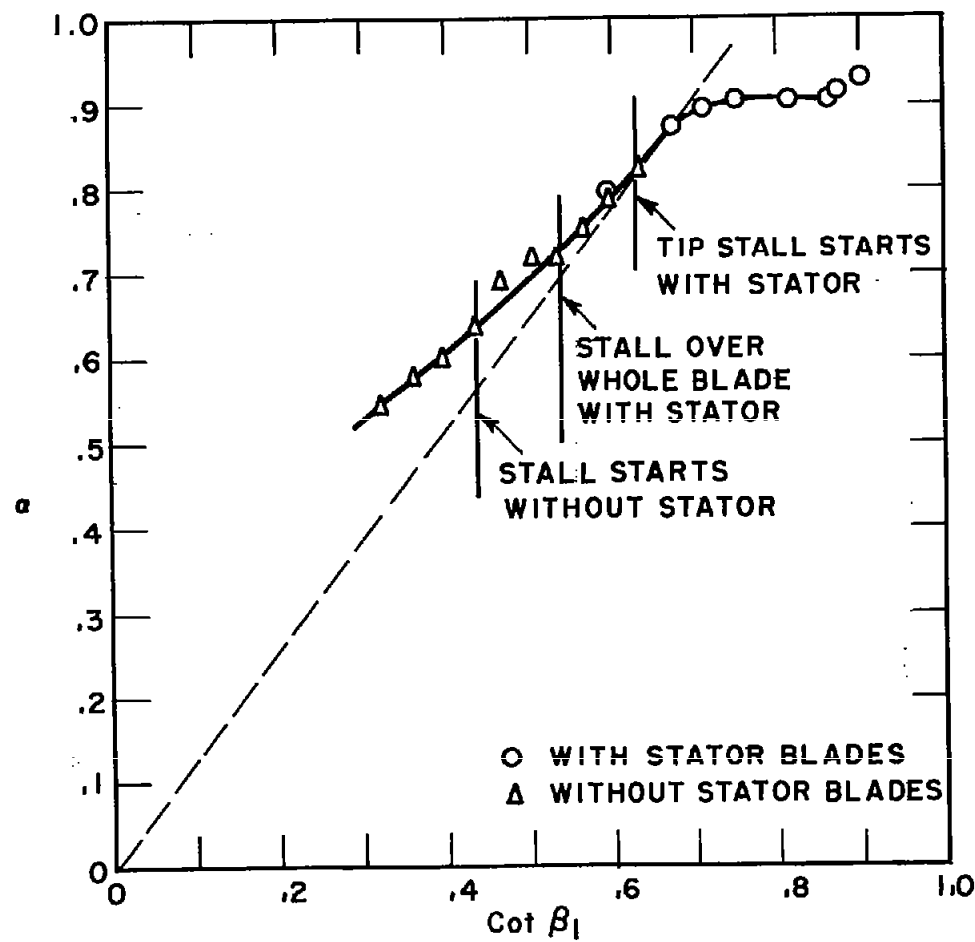
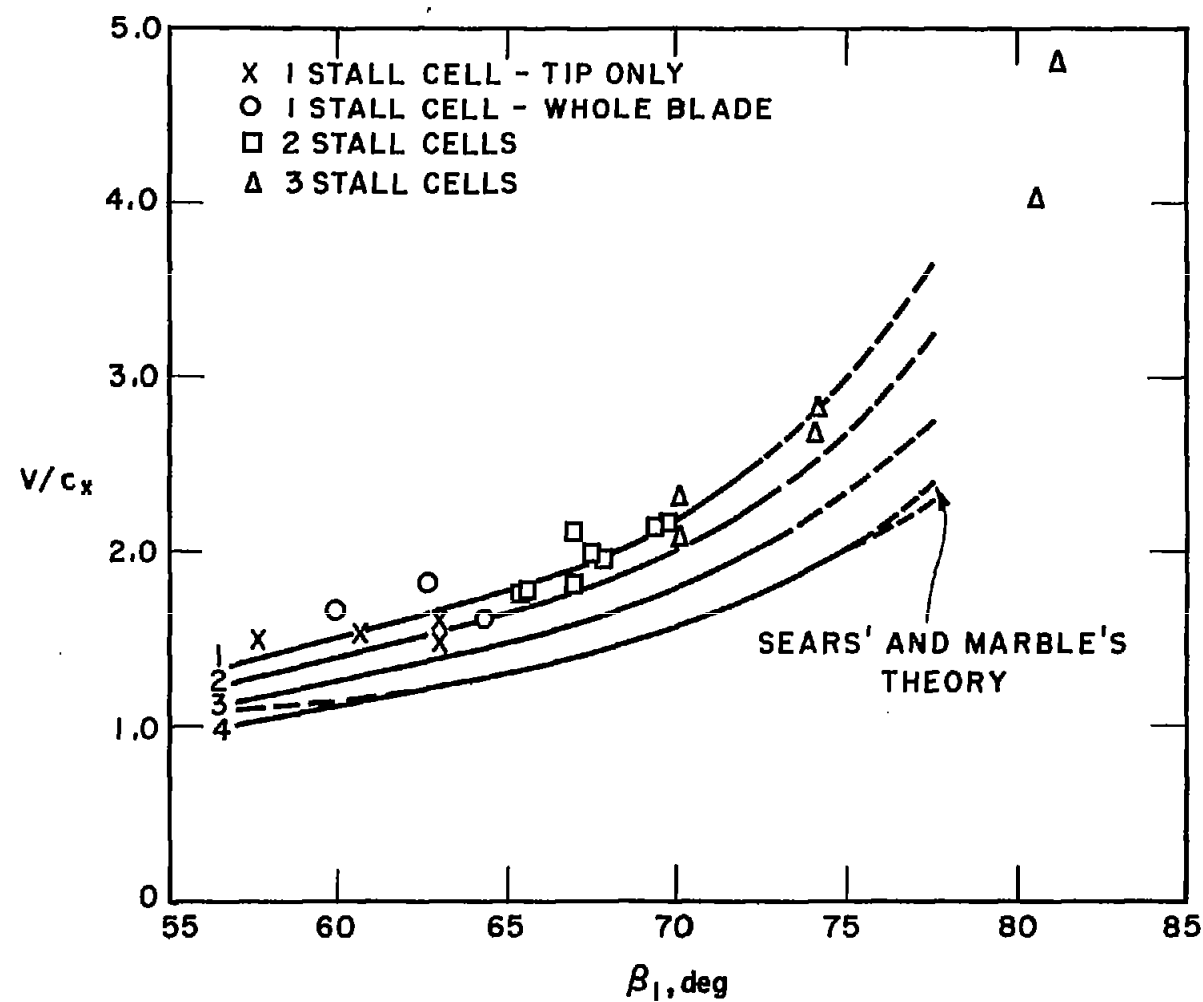


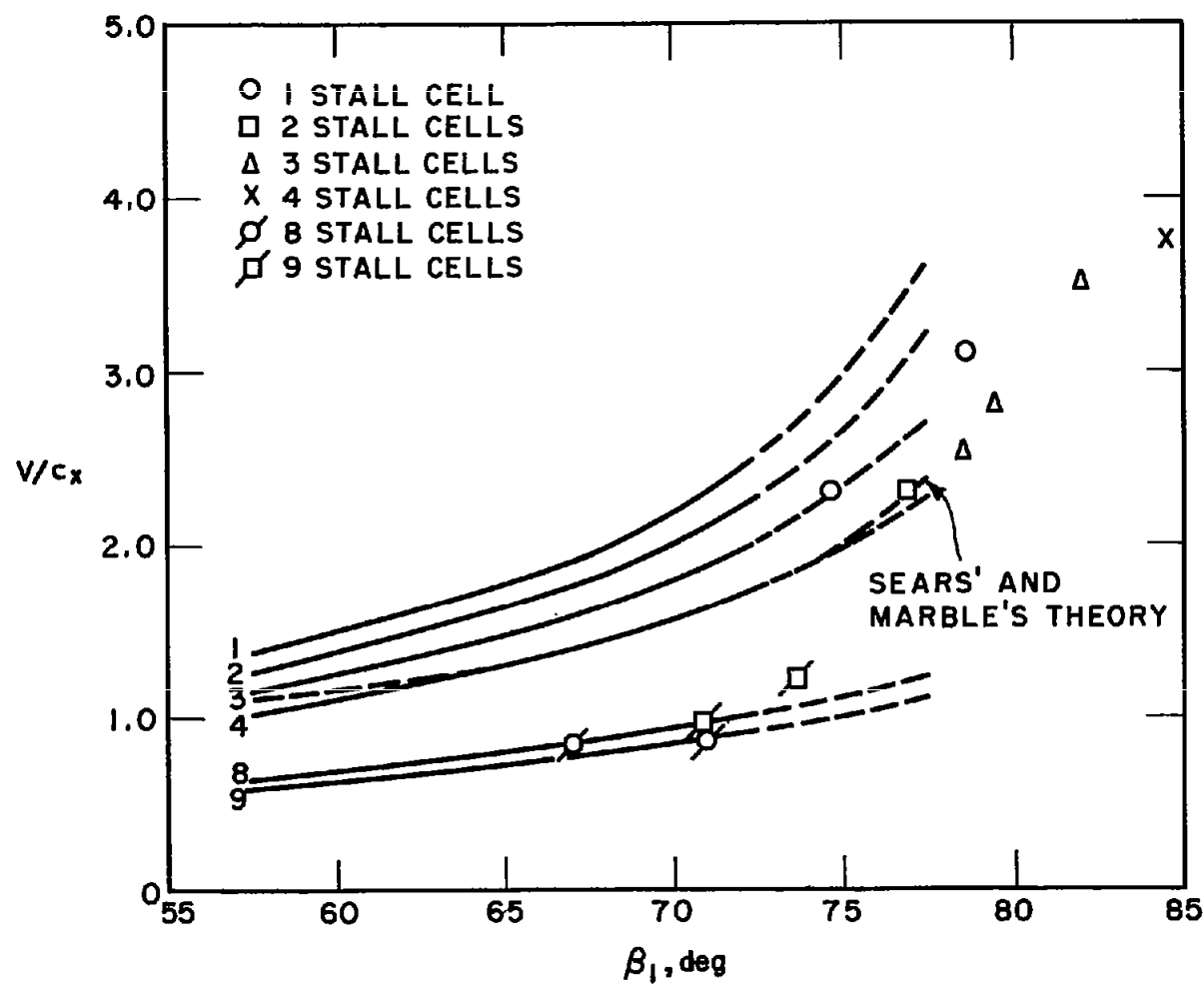
Figure 7.- Blockage coefficient  $\alpha$  against  $\cot \beta_1$ .

$$\alpha \approx A/A' = \frac{\cos \beta_1}{\cos \beta_2 \sqrt{1 - c_p}}$$



(a) With stator blades.

Figure 8.- Stall propagation velocities  $V/C_x$  against  $\beta_1$ .



(b) Without stator blades.

Figure 8.- Concluded.